J. of Supercritical Fluids 55 (2010) 510–523

Contents lists available at ScienceDirect

The Journal of Supercritical Fluids

journal homepage: www.elsevier.com/locate/supflu

Adsorption of N_2, CH_4, CO and CO_2 gases in single walled carbon nanotubes: A combined experimental and Monte Carlo molecular simulation study

George P. Lithoxoos[a,b], Anastasios Labropoulos[c], Loukas D. Peristeras[b], Nikolaos Kanellopoulos[c], Jannis Samios[d,**], Ioannis G. Economou[a,e,*]

[a] National Center for Scientific Research "Demokritos", Institute of Physical Chemistry, Molecular Thermodynamics and Modelling of Materials Laboratory, GR-15310, Aghia Paraskevi Attikis, Greece
[b] Scienomics, 17 square Edouard VII, 75009, Paris, France
[c] National Center for Scientific Research "Demokritos", Institute of Physical Chemistry, Membranes for Environmental Separations Laboratory, GR-15310, Aghia Paraskevi Attikis, Greece
[d] National and Kapodistrian University of Athens, Department of Chemistry, Laboratory of Physical Chemistry, Panepistimiopolis, 15771, Athens, Greece
[e] The Petroleum Institute, Department of Chemical Engineering, PO Box 2533, Abu Dhabi, United Arab Emirates

ARTICLE INFO

Article history:
Received 31 May 2010
Received in revised form
11 September 2010
Accepted 15 September 2010

Keywords:
Single wall carbon nanotubes (SWCNTs)
Grant canonical Monte Carlo (GCMC) simulations
Gravimetric gas adsorption measurements

ABSTRACT

In this study, the adsorption capacity of single-wall carbon nanotubes (SWCNTs) bundles with regard to the pure CH_4, N_2, CO and CO_2 gases at 298 K and pressure range from 0.01 up to 2.0 MPa has been investigated experimentally and computationally. Experimental work refers to gravimetric surface excess adsorption measurements of each gas studied in this nanomaterial. Commercial samples of pristine SWCNTs, systematically prepared and characterized at first, were used for the evaluation of their adsorption capacity. A Langmuir type equation was adopted to estimate the total adsorption isotherm based on the experimental surface excess adsorption data for each system studied. Computational work refers to Monte Carlo (MC) simulation of each adsorbed gas on a SWCNTs model of the type (9, 9) in the grand canonical (GC) ensemble at the same conditions with experiment using Scienomics' MAPS platform software simulation packages such as Towhee. The GCMC simulation technique was employed to obtain the uptake wt% of each adsorbed gas by considering a SWCNTs model of arrays with parallel tubes exhibiting open-ended cylindrical structures as in experiment. Both experimental and simulation adsorption data concerning these gases within the examined carbon material are presented and discussed in terms of the adsorbate fluid molecular characteristics and corresponding interactions among adsorbate species and adsorbent material. The adsorption isotherms obtained exhibited type I (Langmuir) behavior, providing enhanced gas–substrate interactions. We found that both the experimental as well as the simulated adsorption uptake of the examined SWCNTs at these conditions with regard to the aforementioned fluids and in comparison with adsorbate H_2 on the same material increase similarly and in the following order: $H_2 \ll N_2 \approx CH_4 < CO \ll CO_2$. Furthermore, for each adsorbate fluid the calculations exhibit somewhat greater gas uptake with pressure compared to the corresponding experiment. The difference in the absolute uptake values between experiment and simulation has been discussed and ascribed to the following implicit factors: (i) to the employed model calculations, (ii) to the remained carbonaceous impurities in the sample, and (iii) to a proportion of close ended tubes, contained in the experimental sample even after preparation.

1. Introduction

The global warming effect and its severe consequences, as observed through the detrimental alterations in the climate and natural environment of our planet undoubtedly give rise to alerting predictions and concerted actions worldwide. Additionally, the emission of certain well-known flue-gases, such as nitrogen and carbon oxide, involves harmful effects for both our environment and the human health. On the other hand, the rapidly expanding energy requirements, together with the gradual depletion of the fossil fuels reserves imply the necessity for the development of

* Corresponding author at: National Center for Scientific Research "Demokritos", Institute of Physical Chemistry, Molecular Thermodynamics and Modelling of Materials Laboratory, GR-15310, Aghia Paraskevi Attikis, Greece. Tel.: +30 2106503963.
** Corresponding author.
E-mail addresses: isamios@chem.uoa.gr (J. Samios), economou@chem.demokritos.gr (I.G. Economou).

0896-8446/$ – see front matter © 2010 Elsevier B.V. All rights reserved.
doi:10.1016/j.supflu.2010.09.017

Nomenclature

SWCNT	single walled carbon nanotube
wt%	weight percentage of the adsorbed gas in carbon nanotubes
V	volume of the vapor adsorbed
V_o	maximum volume of adsorption in micropores
E_o	characteristic energy of adsorption of a reference vapor
β	similarity or affinity coefficient
n	heterogeneity factor
D	nanotube diameter
H	nanotube height
L_1, L_2, L_3	lateral dimensions of the simulation cell
g	intertube distance
T_c	critical temperature
μ_e	permanent electric dipole moment
Q_m	quadrupole moment
d_k	kinetic diameter
$T_r = T/T_c$	reduced temperature

new strategies with regard to the energy sources production and exploitation of their energy content.

Among the available storage technologies for H_2 and other gases, physical and chemical sorption on solid sorbents is possibly the most appropriate and efficient choice. A promising solid sorbing material has to exhibit a variety of unique physical and chemical properties: (a) sufficient storage capacity for a given gas at room temperature, (b) fast and quantitative recovery of the adsorbed gas without any need to increase the temperature, (c) chemical stability and (d) low cost of preparation and operation. Furthermore, it is essential for the sorbent to be as light as possible with no large available volume requirements (i.e. to exhibit high volumetric density of the adsorbed phase). Physical adsorption, for instance, on the surface of porous materials exhibiting high specific surface area could be an alternative for H_2 storage with the potential to meet the storage requirements designated by the US Department of Energy (DOE) (gravimetric adsorption capacity of H_2 6.5 wt%, or 65 g H_2/kg C), for the year 2010 [1].

To this point, after the discovery of carbon nanotubes (CNTs) [2] and carbon nanofibers [3,4], much attention has been devoted to their potential applications, such as the possible storage of H_2 [5], capture of CO_2 [6] from emitted flue-gases and separation or purification of natural gas and other gaseous mixtures gaseous mixtures [7] via selective adsorption of a specific component. Experimental and theoretical studies devoted to the investigation of the possible mechanisms of H_2 adsorption on various types of CNTs have been also reported in the literature [8–25]. However, although numerous encouraging results have been published on this topic in recent years, it is clear that further thorough efforts are needed to explore the precise physicochemical adsorption mechanism of H_2 in this kind of material. Specific details on the aforementioned problem were thoroughly presented and discussed in recent publications (see for instance Refs. [19,20,25]).

On the other hand, single-wall carbon nanotubes (SWCNTs) bundles might be used for adsorption of a variety of other gases such as CH_4, N_2, CO_2 and CO at supercritical (SC) temperatures. Adsorption of SC gases on SWCNTs bundles is an issue of major importance concerning both fundamental research and various applications since it could provoke the development of novel gas storage technologies, with beneficial effects for industries and environment. An alternative application of CNTs might employ membranes for separation of gas mixtures. For instance, CNTs arrays grown inside nanoporous channels of ceramic or zeolitic substrates may constitute thin separation layers on the surface of composite inorganic membranes. Those composite membranes might be studied for separation of mixtures of the aforementioned gases. These separations are basic process stages for the production of a variety of fuels and materials in refineries and polymer industries.

In our previous work [18,26,27] we studied adsorption of H_2 on a certain type of carbon and carbon/silicon SWNTs by employing statistical mechanical Monte Carlo (MC) simulations and quantum mechanical DFT computational techniques. Concretely, combined ab initio and grand canonical MC techniques simulations have been performed to investigate the dependence of hydrogen storage in SWCNTs on both tube curvature and chirality. The *ab initio* calculations at the density functional level of theory (DFT) have provided useful information about the nature of hydrogen adsorption in SWCNT selected sites and the binding under different curvatures and chiralities of the tube walls. Further to this, the grand canonical MC atomistic simulation performed on large-scale nanotube systems with different curvature and chiralities yielded their storage capacity by calculating the weight percentage of the adsorbed material (gravimetric density) under thermodynamic conditions of interest. In the earlier studies, we found that the nanotube's curvature plays an important role in the storage process while the chirality of the tube has no effect [18]. Furthermore, a similar multiscale theoretical approach was used for the investigation of H_2 storage in silicon–carbon nanotubes (SiCNTs). First, ab initio calculations at the DFT level showed an increase of 20% in the binding energy of H_2 in SiCNTs compared with pure carbon nanotubes (CNTs). This was explained by the alternative charges that exist in the SiCNT walls. Second, classical MC simulation of nanotube bundles showed an even larger increase of the storage capacity in SiCNTs, especially in low temperature and high pressure conditions. In the present study, our effort on this field is extended to investigate experimentally and theoretically the adsorption of the pure CH_4, N_2, CO_2 and CO gases in SWCNTs bundles by using appropriate techniques.

Although numerous experimental studies have been carried out to obtain physical adsorption isotherms of several pure gases on different porous solids over a wide range of thermodynamic conditions [6,16,28–31], the majority of them is directly related to the excess surface adsorption isotherms and only a few studies were devoted to determine the total or absolute adsorption isotherms [32]. We mention also that the surface excess adsorption results cannot serve for comparison with theoretical predictions derived from MC computer simulations and density-functional theory (DFT) statistical mechanical theoretical techniques. Therefore, a necessity arises to employ a method for the calculation of total adsorption isotherms based on experimental surface excess adsorption data obtained over a given gas phase pressure regime. However, the method required for the indirect determination of total adsorption should take into account the incapability of various equations of state describing vapor physisorption, to provide explicit information on adsorption at SC temperatures, without being appropriately modified.

In this treatment, from the experimental excess adsorption isotherms of these gases, the corresponding absolute adsorption isotherms were calculated. On the other hand, the absolute adsorption results from simulations of these systems were directly compared with the corresponding calculated absolute adsorption isotherms derived from the experimental adsorption data in order to explain specific features of the predicted adsorption behavior.

By considering the computer simulation studies reported on the field so far, it should be mentioned that for the study of the gas adsorption isotherms for such materials, the most appropriate method is the grand canonical MC (GCMC) simulations. Furthermore in some cases the molecular mechanics (MM) and molecular dynamics (MD) simulation techniques were also employed to explore specific problems to this interesting topic. Thus, the adsorp-

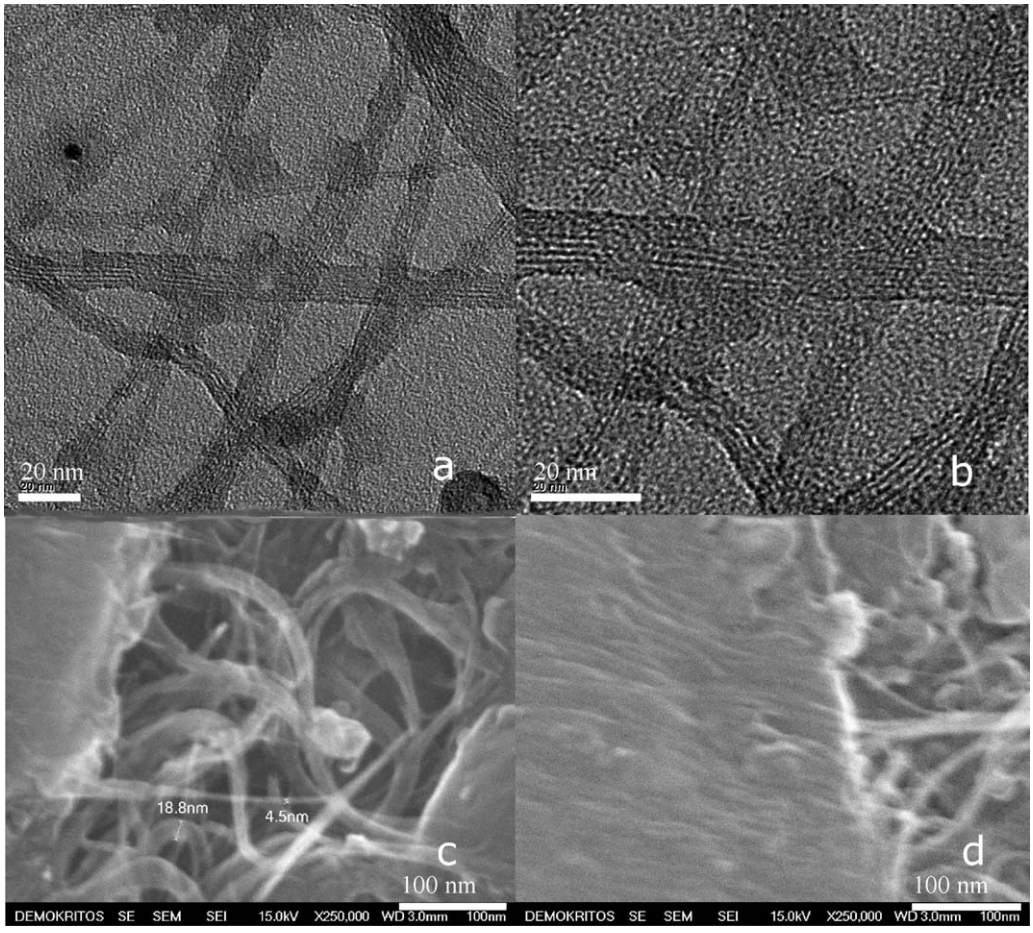

Fig. 1. (a and b) TEM micrographs of the commercial sample of pristine SWCNTs, (c and d) SEM micrographs of the specific sample.

tion capacity of SWCNTs bundles with respect to the pure gases of CH_4, N_2, CO, CO_2 and in comparison to the corresponding data of H_2 at 298 K, was investigated by means of NVT and grand canonical MC model simulations, employing a chirality of (9,9) armchair tubes. The study of intermolecular interactions between gases and nanotube surface was based on potential models from the literature. This effort was combined with gravimetric adsorption experiments of the aforementioned gases at 298 K and pressures up to 2 MPa to determine the surface excess adsorption uptake of each gas on a commercial sample of pristine SWCNTs, systematically treated and characterized prior to the adsorption measurements.

The rest of the paper is organized as follows: In Section 2, we present the experimental methodology used to prepare and characterize the commercial sample of commercial pristine SWCNTs and to obtain the excess adsorption isotherms of the adsorbate gases. In Section 3, we describe the theoretical method employed to determine the absolute gas adsorption isotherms from the excess ones. In Section 4, we give details of the GCMC simulations of the investigated systems. In Section 5, we present and discuss both our experimental and simulation results, and finally, in Section 6, we summarize our main findings.

2. Experimental methodology

2.1. Carbon nanotube sample pretreatment

The pristine SWCNTs used in this work were purchased from Carbon Solutions. According to the manufacturer specifications, the nominal distribution of outer diameters was centered at 1.4 nm with a length distribution between 0.5 and 1.5 μm, while their end-cups have been removed by a purification procedure. Moreover, the purity of the sample was estimated to be approximately 80 wt%, whereas the impurities consisted of metal catalyst particles (∼6.5 wt%, as determined by TGA analysis) and several other carbon nanostructures.

The commercial sample of pristine SWCNTs was subjected to a mild oxidation treatment using air stream with a flow rate of 150 ml/min at 400 °C, for a period of 15 min. The oxidation process aimed to the removal of amorphous carbon impurities as well as the partial opening of closed SWCNTs hemispherical caps. The purification of the commercial sample leads to an increase of the number of available adsorption sites on carbon nanotube surface, which was expected to enhance the capability of the oxidized sample to adsorb several gases. Furthermore, the oxidized sample was thermally treated up to 900 °C, with a heating rate of 5 K/min followed by an isothermal step at this temperature for a period of three hours, under an argon stream flow with a flow rate of 150 ml/min. The annealing process was conducted in order to completely open the remaining SWCNTs closed caps, together with the drastic removal of bulky carboxylic groups, which are located at the edges and possible sidewall defects of carbon nanotubes. Those groups have been formed by the purification treatment applied to the as-produced raw sample (–COOH groups in the purified commercial sample had a nominal ratio of ∼6% per carbon atom) and during the following oxidation treatment of the commercial sample. The closed nanotubes half-fullerene tips exhibit significant strains and therefore, can be readily oxidized and open by means of a simple acid treatment. Thus, the actual density of –COOH groups formed at the open ends is significantly higher than the overall percentage of 6% per carbon atom. Since a large number of free bulky carboxyl

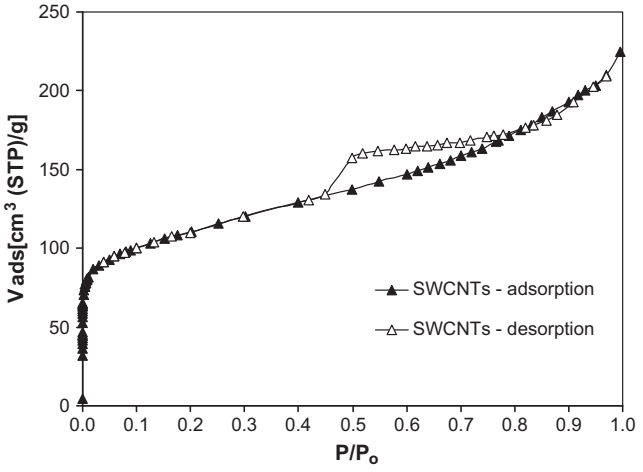

Fig. 2. Experimental N_2 adsorption–desorption isotherm for oxidized–annealed SWCNTs at 77 K.

groups is confined at the narrow open ends (with a diameter of few angstroms), these groups severely prevent the entrance of adsorbate species into the nanotube inner (endohedral) adsorption sites [33,34]. Therefore, the annealing process aimed to further facilitate the access of gaseous molecules into the interior space of the opened carbon nanotubes. The obtained oxidized–annealed sample was used for the evaluation of the SWCNTs adsorption capacity with respect to the aforementioned gases.

2.2. Characterization and adsorption measurements

2.2.1. Transmission electron microscopy

The sample of the CNTs was characterized by employing the *transmission electron microscopy* (TEM) technique. Thus, prior to characterization and use, the sample was prepared by extensive sonication of the CNTs in high-purity ethanol. A drop of the solution was deposited onto a Lacey C-film supported on a Cu grid and the solvent was allowed to evaporate in air. TEM analysis was then carried out in a JEOL 2011 HR-TEM, operating at 200 kV and fitted with an Oxford Instruments INCAx-sight EDS detector. Note that a Scanning Electron Microscopy (SEM) micrograph of the sample was also detected in order to obtain supplementary information regarding the NT structure. The micrographs derived from TEM and SEM microscopy are depicted in Fig. 1a–d and the morphology obtained is discussed in Section 5.

2.2.2. Nitrogen adsorption porosimetry

The porous structure of both the pristine and the oxidized–annealed SWCNTs sample was examined by means of N_2 porosimetry. In each case the corresponding sample was loaded in a narrow glass tube and heated at 573 K under vacuum, for 24 h. A nitrogen adsorption–desorption isotherm at 77 K was measured with the Quantachrome Autosorb-1 MP volumetric apparatus. The amount adsorbed at each relative pressure (P/P_o, where P is the pressure of nitrogen vapor and P_o is the saturation pressure of N_2 at 77 K) was obtained by admitting appropriate volumes of ultra high purity (99.9995%) nitrogen gas into the sample cell at 77 K and measuring the equilibrium vapor pressure. The N_2 adsorption–desorption isotherm for the oxidized–annealed SWCNTs at 77 K is shown in Fig. 2.

Analysis of the adsorption and desorption data was carried out to investigate the mesoporous and microporous structure of the sample. The Brunauer–Emmett–Teller (BET) [35] method was applied to determine the BET surface area (S_{BET}) and the adsorbent monolayer capacity (v_m). The linear plot of the BET method included seven points in the P/P_o region between 0.049 and 0.126. The volume of mesopores (V_{meso}) and their size distribution (PSD) was obtained by applying the Barrett–Joyner–Halenda (BJH) analysis to the isotherm desorption branch. Moreover, V_{meso} was estimated by the difference between the adsorbed volume at $P/P_o = 0.97$ (i.e. $V_{0.97}$) and the total volume of micropores plus ultramicropores of the SWCNTs bundles i.e. $V_{0.97} - (V_{micro} + V_{ultramicro})$. In both cases, the calculation results for V_{meso} were almost identical. Micropore analysis in the relative pressure region of $\sim 2 \times 10^{-4}$ to 0.059 was conducted by the Dubinin–Astakov (DA) method, to determine the micropore volume (V_{micro}) and micropore size distribution. The DA expression can be considered as an expansion of the well-known Dubinin–Radushkevich (DR) equation, which describes adsorption by microporous solids. The DR theory assumes a Gaussian-type micropore potential energy distribution and can be expressed by the following equation [36–40]:

$$\frac{V}{V_o} = \exp\left[-\left\{\left(\frac{RT}{\beta E_o}\right)\cdot \ln\frac{P_o}{P}\right\}^2\right] \quad (1)$$

V is the volume of the vapor adsorbed and V_o is the maximum volume of adsorption in micropores (corresponding to their total volume filling). E_o is the characteristic energy of adsorption of a reference vapor (usually benzene), while β is the similarity or affinity coefficient which can be calculated by the physical properties of the adsorptive and a standard vapor (benzene). The DR equation is effectively applied for the description of adsorption of vapors by materials with a homogeneous microporous structure [36,40].

According to the DA adsorption model [41,42], micropore filling is described by the following equation:

$$\frac{V}{V_0} = \exp\left[-\left\{\left(\frac{RT}{\beta E_o}\right)\cdot \ln\frac{P_o}{P}\right\}^n\right] \quad (2)$$

where n is an additional parameter related to the normalized form of a Weibull distribution function of the differential molar work of adsorption and has been referred to as a "heterogeneity factor". The DA equation takes into account the heterogeneity of the micropore structure of the adsorbent due to the presence of micropores of different size. Therefore, it can be considered as a more generalized expression of adsorption isotherm with regard to the DR equation, being equivalent to the later when $n = 2$. Carbon adsorbents with relatively uniform micropores of molecular dimensions exhibit values of $n > 2$, whereas values of $n < 2$ have been found for activated carbons, with a broad micropore size distribution [43,44]. The results obtained from the N_2 porosimetry are presented and discussed in Section 5.1.

2.2.3. Gas adsorption isotherms

An automated gravimetric sorption analysis apparatus of HIDEN Analytical (*intelligent gravimetric analyzer*, IGA) was used to obtain adsorption isotherms of ultra high or high purity N_2 (99.9995%), CH_4 (99.95%), CO (99.98%) and CO_2 (99.998%) gases conducted at 298.15 K. The equilibrium pressures ranged from 0.01 up to 1.9 MPa in the case of N_2 and up to 2.0 MPa for CH_4, CO and CO_2. Supplementary measurements were also carried out for H_2 at the same conditions. Prior to measurements, the sample cell was out gassed at 573 K until a pressure of 1×10^{-6} mbar was reached. Upon completion of degassing, the initial sample mass was measured. Then, the sample chamber was thermally equilibrated at the temperature of measurements and appropriate gas pressure increments were released into the chamber to reach the selected equilibrium pressures. The increase of sample mass due to adsorption was continuously recorded until equilibrium of the adsorption system was attained and then, the final mass of adsorbent plus adsorbate was obtained. The resolution of the measurements was ±0.1 μg. The results obtained are presented and discussed in Section 5.1.

3. Absolute adsorption isotherms-theoretical background

3.1. Absolute amount adsorbed: general considerations

It is well known that the capability of porous solids to adsorb gases (or vapors) can be deduced by two different types of adsorption isotherms, namely the Gibbsian surface excess and the total (or absolute) adsorption ones. The surface excess adsorption (SEA) at a given temperature is defined as the quantity of a gas (or vapor) required to be introduced into a completely evacuated space of a certain volume, which contains the solid adsorbent, so that the gas phase to reach a given equilibrium pressure minus the quantity of the specific gas (or vapor) required to be supplied into the same evacuated system in order to attain the same equilibrium conditions, if no adsorption would occur. The difference between the total and the excess adsorption stems from the fact that the number of molecules not interacting with the adsorbent surface is smaller than the respective number of molecules in the case that no adsorption on the surface occurred. Thus, the difference arises from the number of gas (or vapor) molecules interacting with the solid adsorbent and is expressed by the volume of the adsorbed phase.

The excess adsorbed amount, n_{ex}, in mol g^{-1} is directly determined by means of gas adsorption experiments (either volumetric or gravimetric). The experimentally determined adsorption isotherms are the ESA isotherms. These isotherms exhibit a characteristic maximum at a certain equilibrium pressure, followed by a downward straight line at higher pressures [45–49]. On the other hand, the total adsorbed amount, n_{ab}, cannot be directly determined. The total amount of a gas contained in the inhomogeneous phase of the gas–solid adsorbent system as a function of the gas phase pressure at a given temperature, i.e. the total adsorption (TA) isotherm (which has to be determined from the excess one) is characterized by a monotonous increase of the adsorbed quantity with increasing pressure [50].

If $\rho_{ad}(r)$ describes the density of the TA at any position r within the volume V_{ad} of the adsorbed phase, then the TA amount is determined by integration of the density with respect to the whole volume of the adsorption space. The fundamental difficulty with this definition is the choice of the volume of the adsorbed phase used in the integration. For small micropores, where the potential force fields of the two opposite walls overlap, the density of the adsorbed phase everywhere will be greater than the adsorbate bulk density. In such cases one can choose the volume of the adsorbed phase as the micropore volume and calculate the absolute amount as:

$$n_{ab} = \int_{V_{micro}} \rho_{ad}(r)\, dr \tag{3}$$

where V_{micro} is the micropore volume. The problem of the definition of the adsorbed phase volume arises for porous solids possessing a pore size distribution. The relation between the total adsorbed amount, n_{ab}, and the excess adsorbed amount, n_{ex}, is given by the following equation:

$$n_{ab} = n_{ex} + \rho_b \cdot V_{ad} \tag{4}$$

where $\rho_b (= \rho_{bulk})$ is the gas phase bulk density. When adsorption measurements are performed, the amount n_{ex} and ρ_b can be determined. On the other hand, the quantities n_{ab}, V_{ad} and $\langle \rho_{ad} \rangle$ – where $\langle \rho_{ad} \rangle$ represents the average density of the adsorbed phase – can not be directly determined. It is noted that those three quantities refer to the total (absolute) adsorption in contrast to the excess ones. It is obvious that the estimation of n_{ab} requires the calculation of the corresponding V_{ad} or $\langle \rho_{ad} \rangle$ values, which cannot be experimentally measured but only approximated by means of Helium adsorption experiments. Gumma and Talu [51] have proposed a method to approximate adsorbed volume in microporous systems.

The SC fluids cannot coexist with their liquid phase in contrast with vapors. When the gaseous adsorbates are in the vapor phase (i.e. at subcritical temperatures) they tend to form a complete adsorbed monolayer on the surface of solid adsorbents or complete the stage of micropore filling in the case of micropores existence. Upon completion of the monolayer coverage, multilayer adsorption might follow on the surface of non-porous or macroporous solids at higher vapor phase pressures, whereas capillary condensation occurs as a consequence of a coexisting mesoporous structure. The shape of the corresponding adsorption isotherms and the evolution of the adsorbed layer formation depend on the interactions between vapor molecules and porous or non-porous adsorbent surface with respect to the vapor phase intermolecular forces. In all cases, at subcritical temperatures the adsorption of vapors is completed at a pressure equal to the saturation vapor pressure, P_o, of the adsorbate. Therefore, each subcritical adsorption isotherm can be derived in the form of adsorbed amount (or volume) of vapors as a function of the relative pressure, P/P_o, of the adsorbate. On the other hand, the saturation vapor pressure is meaningless for gases being at temperatures higher than their critical temperature, T_c. Consequently, the models describing physisorption of vapors, including multilayer adsorption and capillary condensation (BET theory, Kelvin equation and t-plots) can not be applied for the description of physisorption of SC gases.

The fact that the close proximity between total adsorption and surface excess adsorption isotherms is limited to sub atmospheric pressures, along with their growing mutual deviation when adsorption occurs at higher pressures, results in certain restrictions. Although surface excess adsorption data determined for several solid adsorbents is suitable for industrial applications, such as separation of air or flue gases components and purification of natural gas, however it is inappropriate for calculation of relevant thermodynamic functions. Furthermore, at SC temperatures, SEA isotherms cannot be fitted to various models describing adsorption on homogeneous (in terms of adsorption enthalpy, i.e. Langmuir isotherm) and heterogeneous solid adsorbents (e.g. Sips or Toth isotherm). Therefore those models are not reliable for assessment of the saturation adsorption capacity as well as to investigate the porous structure of solid adsorbents. Moreover, the SEA results cannot serve for comparison with theoretical predictions derived from GCMC simulation and statistical mechanical DFT calculations. Therefore, a necessity arises to employ a method for the calculation of the TA isotherms based on experimental SEA data obtained over a given gas phase pressure regime.

3.2. Adsorption of supercritical gases

It should be assumed that the microporosity is able to induce physisorption of SC gas molecules by means of gas–micropore interactions, even though the adsorbed phase concentration is relatively suppressed at low to moderate pressures. Nevertheless, under high equilibrium pressures the adsorbed molecules concentration is increased and their mutual interactions become important. Specifically, it can be assumed that the interaction potential inside narrow micropores is attractive enough to provoke a high degree of micropore filling, resulting in a high concentration of the adsorbed molecules [52–54]. The increase of the adsorbed phase density is followed by a gradual decrease of the adsorbate mobility. In general, whereas narrower micropores can be filled with SC adsorbate molecules, the larger micropores will accommodate usually at most a two dimensional monolayer. Formation of an additional loosely packed and quite mobile adsorbed layer is possible at either very high pressures or at a temperature close to the critical one. Thus, the SC gas adsorbed within micropores can be transformed into a mobile single or a two-dimensional monolayer

with restricted freedom for molecular translational movements or into a so-called quasi-vapor, depending on the micropore width, which determines the interaction potential energy and the available pore volume [55]. The onset of lateral interactions results in a progressively increasing deviation between the SEA isotherm and the corresponding Langmuir adsorption isotherm. The behavior of the SEA isotherm at high pressures has been attributed to strong repulsive interactions between adsorbed molecules due to their close packing, which compensate for the attractive forces exerting to the adsorbent surface. At those pressures, the gas phase bulk density approximates the absolute density of the adsorbed phase and the SEA isotherm tends to intercept the gas pressure axis at a certain pressure, for which the excess density of the adsorbed phase is zero ($\langle\rho_{ex}\rangle = 0$ and $\langle\rho_{ad}\rangle = \rho_b$).

The transition of the adsorbed phase into a quasi-vapor state inside wider micropores might progress via the typical micropore filling mechanism, which has been described by Dubinin and et al. [37,41]. A saturated quasi-vapor state could arise as soon as the average density of the adsorbed phase is reached by the bulk density as the equilibrium pressure increases. Taking into account the looser "average" packing of the adsorbed molecules, which corresponds to the average density of the saturated adsorbed phase inside wider micropores, in comparison to their closest packing within a very restricted micropore space, it can be deduced that the equivalent volume of the saturated "close packing" quasi-vapor, V_{sat}, is lower than the total micropore volume, V_m. The Langmuir model (describing adsorption isotherms of type I) can also be adopted for the representation of the total adsorption isotherm:

$$\theta = \frac{n}{n_m} = \frac{KP}{1+KP} \tag{5}$$

where θ is the surface coverage, n is the adsorbed amount and n_m and K are the saturation adsorption capacity and the Langmuir adsorption coefficient, respectively. This approach relies on the stronger adsorbate–solid adsorbent interactions in comparison with the adsorbate lateral interactions at SC temperatures and low equilibrium pressures.

3.3. Ono–Kondo equations for the description of excess adsorption.

Physisorption of SC gases onto the SWCNTs endohedral sites at low to moderate pressures can be approached with regard to monolayer coverage of the walls of cylindrical nanopores, having a diameter of at most 20 Å. A similar case of physical sorption has been studied for slit-shaped pores of activated carbons [58]. Each graphitic nanotube incorporates distinct adsorption sites with a periodic spatial arrangement, which formulates the arrangement of the adsorbed molecules, based on the assumption that each adsorption site can be occupied by solely one adsorbate molecule. Therefore, the lattice of the adsorbed molecules within the cylindrical nanopore will be constituted of a concentric hexagonal shell. The molecular fraction per adsorption site x_i on the adsorbate layer is related to the molar density ρ_i, of the adsorbate by the expression: $x_i = \rho_i/\rho_{mc}$, where ρ_{mc} is the bulk molar density at maximum adsorption capacity, corresponding to the complete monolayer coverage. The surface excess adsorption amount, n_{ex}, is given by: $n_{ex} = C(x_i - x_b)$. The molecular fraction x_b is equal to ρ_b/ρ_{mc}, where ρ_b is the bulk molar density of the adsorbate (corresponding to ρ_i) and C is a prefactor related to the structural properties of the adsorbent and the cylindrical pore geometry.

In the literature, the well-known Ono–Kondo equations (OKE) have been employed so far in an approach for the theoretical prediction of surface excess gas adsorption isotherms under quite high pressures, at both subcritical and supercritical temperatures [56–59]. The OKE equations are a set of coupled self-consistent non-linear equations describing the density profile of successive layers of adsorbed molecules. The average density of the TA phase, $\langle\rho_{ad}\rangle$ and the average density of the excess part of the adsorbed phase, $\langle\rho_{ex}\rangle$, are given by Eqs. (6) and (7), respectively:

$$\langle\rho_{ad}\rangle = \int_{V_{ad}} \frac{\rho_{ad}(r)\,dr}{V_{ad}} = \frac{n_{ab}}{V_{ad}} \tag{6}$$

$$\langle\rho_{ex}\rangle = \int_{Vad} [\rho_{ad}(r) - \rho_b]\,dr \tag{7}$$

Taking into account only the adsorption potential, E_A (i.e. the interactions between adsorbate molecules and adsorbent surface) and neglecting the interactions between the adsorbate molecules ($E = 0$), the solution of the OKE yields the interactionless excess adsorption amount, $n_{ex,o}$, as a function of the molecular fraction x_b:

$$n_{ex,o} = 2C\frac{x_b(1-x_b)(1-\exp(E_A/kT))}{x_b + (1-x_b)\exp(E_A/kT)} \tag{8}$$

In order to determine the parameters E_A, C and ρ_{mc}, the following linear equation is fitted to the experimental excess adsorption data:

$$Y = aX + b \tag{9}$$

The reduced variables Y and X are expressions of the excess adsorption amount, n_{ex} and the bulk density, ρ_b, as given below:

$$Y = \frac{\rho_b}{N}, \qquad X = \frac{\rho_b}{\rho_{mc} - \rho_b} \tag{10}$$

The fitted parameters α and b are related to the physical parameters of the interactionless excess adsorption isotherm through the equations:

$$a = \frac{\rho_{mc}}{2C(1-\exp(E_A/kT))}, \qquad b = \frac{\rho_{mc}\exp(E_A/kT)}{2C(1-\exp(E_A/kT))} \tag{11}$$

The molar density of a completely filled layer of adsorbed molecules, ρ_{mc}, is first determined by optimizing the correlation coefficient of the linear fit of Eq. (10). The onsite adsorption potential, E_A and the prefactor C can be calculated using Eq. (11).

3.4. Procedure for the calculation of the total adsorption isotherm

A method developed by Murata and Kaneko [59] was employed in this study to determine the TA isotherms of the studied gaseous adsorbates by elaborating experimental excess adsorption data at these conditions. As mentioned above, the volume of the adsorbed phase, V_{ad}, has to be calculated to obtain the TA amount, n_{ab}. The iteration procedure adopted for the calculation of n_{ab} and V_{ad} at each equilibrium pressure is that proposed by Kaneko et al. [50]. In this approach, n_{ab} and V_{ad} are treated as a set of sequences $\{n^{(n)}(P)\}$ and $V_{ad}^{(n)}$. The initial conditions are given by:

$$\rho_{ad} = \langle\rho_{ad}(P_{mc})\rangle \tag{12}$$

$$n_{ab}^{(1)}(P) = n_{ex}(P) \tag{13}$$

$$V_{ad}^{(1)} = \frac{\max(n_{ex}(P))}{\langle\rho_{ad}\rangle} \tag{14}$$

In Eq. (12), P_{mc} represents the gas phase pressure where the SEA isotherm intercepts the pressure axis. The bulk phase molar density, $\rho_b(P)$, increases monotonously with pressure in contrast to $\rho_{ex}(P)$ and at the crossing point, $\rho_b(P_{mc})$ becomes equal to $\langle\rho_{ad}(P_{mc})\rangle$ whereas $\langle\rho_{ex}(P_{mc})\rangle = 0$ and therefore $n_{ex}(P_{mc}) = 0$. It is noted that for each studied gas, P_{mc} represents the respective crossing point of the predicted SEA isotherm obtained by elaborating the available experimental SEA data through the OKE based approach.

The following iteration procedure leads to the calculation of n_{ab} and V_{ad} values:

The constants, n_m and K, are determined via the Langmuir plot:

$$\frac{P}{n_{ab}^{(n)}} = \frac{1}{K^{(n)} n_m^{(n)}} + \frac{P}{n_m^{(n)}} \quad (15)$$

At the first step of the procedure it holds that: $n_{ab}^{(1)} = n_{ex}$, whereas $K^{(n)}$ is the adsorption coefficient and $n_m^{(1)}$ is the adsorption saturation capacity. The linear part of the Langmuir plot can be fitted to a lower pressure regime, $P_{inf} \le P \le P_{sup}$, in order to derive the values of $K^{(n)}$ and $n_m^{(1)}$. The Langmuir adsorption isotherm was adopted for the calculation of the TA isotherms of N_2, CH_4 and CO SC gases and subcritical CO_2, using the experimental SEA data. The Langmuir approach was based on the following assumptions: (i) complete monolayer coverage at saturation of adsorption system, and (ii) negligible intermolecular interactions between adsorbed molecules in comparison with the adsorbate–adsorbent interactions.

The volume $V_{ad}^{(n)}$ is obtained via Eq. (16),

$$V_{ad}^{(n)} = \frac{n_m^{(n)} \cdot P_{mc}}{\rho_b(P_{mc})} \cdot \frac{1}{(1/K^{(n)}) + P_{mc}} \quad (16)$$

using the values of $\rho_b(P_{mc})$ and the Langmuir constants.

The calculation of n_{ab} is based on Eq. (17)

$$n_{ab}^{(n+1)}(P) = n_{ex}(P) + \rho_b(P) \cdot V_{ad}^{(n)} \quad (17)$$

and after that return to step 1. The set n_{ab} is the convergence set of $n_{ab}^{(n)}$ and is equal to: $\{n_{ab}(P)\} = \lim_{n\to\infty} \{n^{(n)}(P)\}$, whereas $V_{ad}^{(n)}$ is equal to $V_{ad} = \lim_{n\to\infty} V^{(n)}$. The linearized Langmuir equation is used in order to fit to the values of $n_{ab}^{(n)}(P)$ calculated after the end of each iteration step, so as to derive the next adsorption isotherm, $n_{ab}^{(n+1)}(P)$.

4. Molecular models and simulation details

In the present study, our effort focused on the experimental and theoretical investigation of the adsorption of pure CH_4, N_2, CO and CO_2 gases in SWCNTs by using appropriate techniques. In this Section, we describe the computational methodology used to explore the capability of these microporous solids to adsorb the aforementioned gases.

To this point, it is well established that the adsorption isotherms of gases on a porous solid adsorbent can be calculated via appropriate numerical molecular simulation techniques as well as statistical mechanical DFT computational methods. For the purpose of this work, the simulation procedure of the adsorption phenomenon of gases in microporous solids such as model CNTs may be summarized in the following two steps.

In the first step, the excess chemical potential of each pure investigated adsorbate gas is calculated at the thermodynamic state points of interest, using previously proposed effective force field models employed to describe the interactions among sorbet molecules. To accomplish the aforementioned task, we used NPT MC simulation and the Widom's [60] test particle method. In the second step, we use GCMC [61] simulation technique to determine adsorption of these gases on an armchair open-ended type SWCNT bundles system based on the assumption that no chemical process occurs and therefore on effective classical simulations.

In the framework of each GCMC simulation, we firstly obtain the density profiles and afterwards the weight percent (wt%) of the adsorbed gas inside and outside the tubes, which indicates the adsorption capacity of the system at the selected thermodynamic states. We recall here that the ideal armchair open-ended cylindrical (9, 9) SWCNT model that was selected to be studied exhibit a diameter of about $D = 1.2$ nm and height $H = 3.5$ nm. The bond length C–C is that of graphite carbon at 0.1421 nm. The simulation cell consists of three rows, of three open-ended tubes each, making up a total of 9 parallel and rigid SWCNTs forming a triangular lattice (see Fig. 3). The tube spacing is $g = 0.34$ nm [10,62–64]. In each case, the lateral dimensions of the simulation cell are $L_1 = L_2 = 3(g + D)$ and $L_3 = H$.

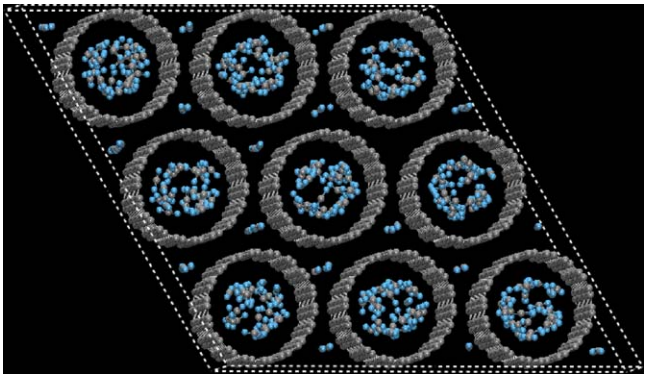

Fig. 3. Snapshot of a simulation box configuration of CO_2 adsorbed on (9, 9) SWCNTs model from the GCMC simulation of the system at 298 K.

4.1. Potential models

Table 1 presents the potential models with the corresponding parameters used for the gas–gas and gas–SWCNT interactions. All the models used are effective potentials which have been optimized and reported by several authors previously as well as employed by others in numerous simulation studies of these molecular systems successfully. In addition, all the models are rigid and therefore contributions from intramolecular effects were not considered, a typical approach applied in computer simulations of simple molecular fluids.

The CH_4 molecules are treated as spherical and rigid particles with one site pair wise LJ (12–6) potential proposed by Saager and Fischer [65]. The N_2 and CO molecules are modeled as diatomic rigid particles with site-site pair wise additive LJ (12–6) potential. The parameter values and other potential details for N_2 are described in a recent simulation study of permeation properties of CO_2 and N_2 through silicalite [[66], see Fig. 2d and Ref. [54]]. In the case of CO, the best-fit potential parameters are taken from a recent simulation study concerning the modeling of CO and other gases adsorption in slit pores using MC technique [[67], see Table 1]. We mention here that the CO employed potential contains electrostatic interactions due to the addition of a small dipole moment that was taken into account represented by a positive and negative point charge on the C and O atom, respectively. The CO_2 was treated as a linear rigid triatomic molecule in its ground state. The molecule–molecule interactions were represented by the EPM2 model [68] that is a three site pair-wise additive LJ (12–6) potential plus an electrostatic part due to the addition of partial charges distributed on the three atoms so as to reproduce the experimental quadrupole moment Q.

In the case of H_2, as in previous studies the sorbate–sorbate interactions are described by a one site Lennard–Jones (LJ 12–6) [10,18] potential model centered on the center of mass (COM) plus electrostatic interactions due to the addition of a quadrupole moment that was taken into account by putting a positive point charge on both hydrogen atoms and a negative one on the COM.

The parameters of the tube carbon–carbon LJ interactions are taken from [10,18]. Note also that in any case the cross LJ param-

Table 1
Lennard–Jones (LJ) potential parameters used in the present simulation study. The cross parameters of unlike pair *i* and *j* interaction sites are obtained by Lorentz–Berthelot (LB) combining rules.

H_2 [10,18]					
$\varepsilon_{H_2-H_2}$	36.7 K	$\sigma_{H_2-H_2}$	2.958 Å	q_H = 0.466e	$q_{com\text{-}H_2} = -0.932e$
N2 [66]					
ε_{N-N}	36.2 K	σ_{N-N}	3.2987 Å		
CO_2 [68]					
ε_{C-C}	28.129 K	σ_{C-C}	2.757 Å	q_C	0.6512e
ε_{O-O}	80.507 K	σ_{O-O}	3.033 Å	q_O	−0.3256e
CO [67]					
ε_{C-C}	22.8 K	σ_{C-C}	3.490 Å	q_C	0.0203e
ε_{O-O}	63.5 K	σ_{O-O}	3.130 Å	q_O	−0.0203e
CH_4 [65]					
ε_{CH_4}	149.92 K	σ_{CH_4}	3.7327 Å		
C–C (in CNTs) [10]					
ε_{C-C}	28.2 K	σ_{C-C}	3.4 Å		

eters of unlike pair *i* and *j* interaction sites are obtained by Lorentz–Berthelot (LB) combining rules.

The simulations in the present treatment were performed at a temperature of 298 K and different pressures in the range 0.01–2.0 MPa using Scienomics' *MAPS* platform and the *Towhee* simulation package [69]. Note that in the case of CO_2 and H_2 we carried supplementary simulations in order to obtain adsorption isotherms at higher pressures and up to about 100 bar. In each NPT MC simulation, corresponding to a different thermodynamic state, we created 2×10^6 MC steps in order to reach system equilibrium and additionally 2×10^6 steps for the calculation of the chemical potential needed for the second part of the procedure. As far as the implementation of the GCMC simulation of a full system is concerned, we performed 10^6 MC steps for the system to reach equilibrium and after that approximately other 10^6 steps spent to obtain statistical averages. The estimated statistical averages of the number of hydrogen molecules inserted and stabilized in the simulation cell for each system and thermodynamic state point of interest are summarized in Table 1 in Supporting information paragraph.

Finally, from the GCMC simulation phase space production run of each investigated system, we have calculated the weight percentage (wt%) of the adsorbed gas molecules as well as their density profile in the system at each state point of interest. The results obtained are presented and discussed in the following section.

5. Results and discussion

5.1. Experimental results

5.1.1. Characterization

The pristine CNTs used in this work were prepared following the procedure described earlier. The CNTs were characterized using the TEM and SEM techniques and by means of N_2 porosimetry and determination of the specific area by the BET method. Fig. 1a and b shows TEM micrographs of the commercial sample of pristine SWCNTs, and Fig. 1c and d shows SEM images of the specific sample. From these micrographs the CNT characteristic structure of the sample is apparent. The derived micrographs from Fig. 1 show SWCNTs bundles having a rather wide diameter distribution, which contain different populations of CNTs. Apart from the crystalline bundles, metallic growth catalyst particles and some other nanostructures such as carbon nanorods and carbon nanorings can also be observed. The average diameter of the SWCNTs bundles was estimated to be equal to 7.14 nm. The average diameter was derived on the basis of an ensemble of 50 countered bundles observed in the micrographs. The estimated value is close to the diameter of a homogeneous bundle consisted of two coaxial SWCNTs shells – an internal and an external shell – which is calculated to be equal to 7 nm, assuming uniform SWCNTs with a diameter of 1.4 nm, according to the geometrical considerations for ideal CNTs bundles reported by Peigny et al. [70]. The geometrically calculated external specific surface area of this ideal bundle is 483.9 $m^2\ g^{-1}$.

Furthermore and according to the experimental protocol, both the pristine and the oxidized–annealed SWCNTs were examined by means of N_2 porosimetry and the corresponding adsorption–desorption isotherms were obtained. From Fig. 2, the N_2 adsorption–desorption isotherm for the oxidized–annealed SWCNT at 77 K was found to be of type IV due to the existence of a hysteric loop and according to the Brunauer, Deming, Deming, and Teller (BDDT) classification [71]. It should be mentioned that the N_2 adsorption–desorption isotherm obtained for the pristine SWCNTs (not shown) exhibits a similar behavior of the type IV. It should be pointed out that the observed isotherm behavior reveals the presence of CNTs in the sample with differences in tube diameters, which are also apparent from the micrographs in Fig. 1. From this point of view, the microporous and mesoporous structure of SWCNTs bundles from the oxidized–annealed sample observed, originate from the stable aggregation of SWCNTs into crystalline ropes, imposed by van der Waals interactions.

It has been pointed out in previous studies that SWCNTs arrange themselves in hexagonal configuration, forming bundles of aligned tubes [72]. Those bundles exhibit heterogeneous porous structure even if they are consisted of similar SWCNTs with uniform tube diameter. Note that according to previous studies, the heterogeneity of both open and closed-ended SWCNTs bundles stems from their multi-shell structure which exhibits discrete groups of adsorption sites with different binding energies [73–76]. In the case of an open-ended CNT bundle, there are four different groups of sites which potentially are available for adsorption. The sites with the lower adsorption energy are the external surfaces of the individual CNTs composing the outermost shell of the bundle. The remaining three groups of adsorption sites are related to higher energies and they are located at (i) the spaces where two neighboring tubes of the outermost shell meet i.e. groove sites, (ii) the spaces between trigonally arranged adjacent tubes (interstitial channels) within the bundle, and (iii) the inner hollow space (endohedral sites) of the individual tubes. Generally, for a given adsorbate, the availability of adsorption sites within the hollow interior space leads to substantial enhancement of the adsorption capacity. The amount adsorbed inside open-ended CNTs is determined mainly by their effective diameter, intrapore potential fields as well as the thermodynamic conditions under investigation [77,78]. SWCNTs with larger diameters have increased effective pore volume, being capable of enclosing more than one layer of adsorbate specimens, especially for the ones with smaller kinetic diameter d_k. In our

Table 2
Pore structure analysis results from this study. The volume of mesopores, V_{meso}, presented in both pristine and oxidized–annealed samples of SWCNTs bundles has been determined by subtraction of the total micropore volume from the total pore volume (i.e. $V_{meso} = V_{0.97} - (V_{micro} + V_{ultramicro})$) and also by the BJH method (i.e. V_{meso} BJH). DR and DA denote "according to the Dubinin–Raduskevich and Dubinin–Astakov method", respectively. All the determined variables are defined in the text.

	$V_{0.97}$ [cm^3 liqN$_2$/g]	S_{BET} [m^2 g^{-1}]	υ_m [cm^3 g^{-1}]	C constant	V_{meso} [cm^3 liqN$_2$/g]	V_{meso} BJH [cm^3 liqN$_2$/g]
SWCNTs pristine	0.267	225.17	0.080	322.2	0.154	0.145
SWCNTs annealed	0.325	397.13	0.141	548.0	0.115	0.120

	V_{micro} (DR) [cm^3 g^{-1}]	V_{micro} (DA) [cm^3 g^{-1}]	E_o [kJ mol^{-1}]	n	$\langle D \rangle$	$V_{ultramicro}$ [cm^3 g^{-1}]
SWCNTs pristine	0.085	0.085	19.63	1.9924	12.9	0.028
SWCNTs annealed	0.154	0.161	21.25	1.8083	12.9	0.049

case, the pristine as well as the oxidized–annealed SWCNTs pore diameter D distribution found to be both centered at $D = 12.9$ Å, as determined via the DA analysis. Note that in this way determined average tube diameter of the pristine and prepared SWCNTs sample has been found systematically smaller compared to the nominal distribution of outer tube diameters centered at 14 Å according to the manufacturer specifications. This experimental result led us to select the ideal single-walled armchair (9, 9) type CNTs bundles model, which exhibits a tube diameter quite close (12.2 Å) to the experimentally estimated one, in order to study the adsorption phenomenon of the aforementioned gases via GCMC computer simulation.

Finally, the results from the porous structure characterization both of the pristine and oxidized–annealed SWCNTs sample in terms of the representative parameters are listed in Table 2. In summary, from the results in this table our treatment upon this material shows clearly that the annealed SWCNTs sample present remarkable enhanced porous structure parameter values compared to the pristine corresponding ones. This may be due to the fact that the removal of impurities and opening of many of the end caps enhance the total specific surface area of the adsorbate material, resulting probably in increased adsorption capacity.

5.1.2. Gas adsorption isotherms

The adsorption capacity of the investigated adsorbate single gases on the sample of oxidized–annealed SWCNTs, under pressures between 0–2 MPa and at 298 K, has been determined by conducting as mentioned above the automatic adsorption analyzer IGA 001.

The experimental excess adsorption isotherms for all the aforementioned gases derived from the gravimetric adsorption experiments, as uptake wt% along with the corrected total (or absolute) adsorption ones according to the calculation procedure described in Section 3, are depicted in Figs. 4 and 5, respectively. Note that despite the purification pretreatment of the pristine sample, a further TGA analysis (thermo-gravimetric) was employed to determine the remaining catalyst substance prior to the conduction of the gravimetric adsorption experiment. Thus, the final total adsorption isotherms were corrected after subtraction of the catalyst mass determined by means of TGA analysis under oxidative conditions up to 1273 K and was equal to 7.4 wt%. It is observed in Figs. 4 and 5 that for the same kind of SWCNTs, the various gas adsorption capacities is substantially increased after the purification and correction procedure employments. Note that the results obtained can be attributed to the increased mass of pure SWCNTs. In general, it is realistic to assume that even some partial removal of the impurities attached to the CNTs surface leads to a larger surface exposition to the adsorbate molecules, improving in this way the gas adsorption uptake. This consideration is in accordance with the SWCNTs characterization results shown in Table 2. The specific surface area and the rest of the characteristic tube properties of oxidized–annealed SWCNTs appeared to be larger than that of the pristine ones.

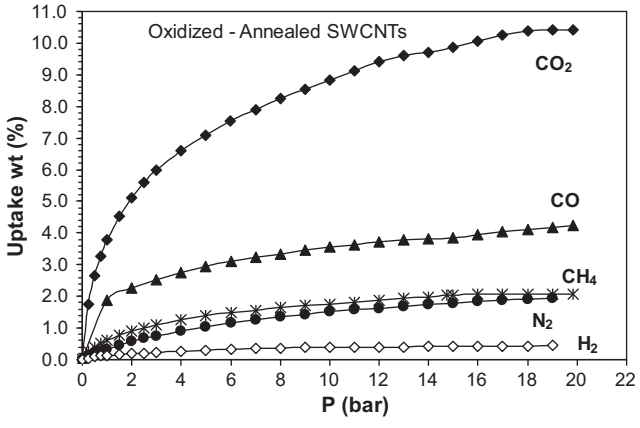

Fig. 4. Experimental gravimetric surface excess adsorption isotherms for the gases H_2, N_2, CH_4, CO and CO_2 on oxidized–annealed SWCNTs, at 298 K.

It must also be emphasized that, certain physicochemical properties of the adsorbate gases listed in Table 3, as the molecular weight, M, critical temperature, T_c, permanent electric dipolar moment, μ_e, quadrupole moment, Q_m and kinetic diameter, d_k [79–81], as well as the reduced temperature of the measurements, $T_r = T/T_c$, affect significantly the adsorption phenomenon in nanomaterials. The kinetic diameter corresponds to the smallest effective dimension of a given molecule, derived from quantum mechanical calculations [82,83] based on either the minimum of the potential energy curve or the distance of equality between attractive and repulsive forces and is taken into account when considering adsorption–diffusion process [84,85]. For non-spherical molecules, for instance, calculations based on this technique refer to their smallest effective waistline diameter. For molecules that are essentially spherical, such as CH_4, Ar, He, etc., d_k is very similar to the gas phase collision or Lennard–Jones diameter. For asymmetric molecules such as CO_2 and N_2, however, the kinetic diameter corresponds more closely to the minimum diameter of the molecule. In transport phenomena, the molecule with the smallest effective waistline diameter is that which diffuses faster and behaves as the smallest one, i.e., the molecule with the smallest kinetic diameter.

On the other hand, it is pointed out based on previous experimental and theoretical studies that in general the gas adsorption onto nanostructure materials obtained at relatively lower temper-

Table 3
Physical properties of the studied adsorbates. The values for the kinetic diameter d_k are taken from the recent literature (see text, Section 5.1).

	H_2	N_2	CH_4	CO	CO_2
M [g/mol]	2.016	28.013	16.043	28.01	44.01
T_c [K]	33.2	126.2	190.6	132.9	304.1
μ [Debye]	0	0	0	0.1	0
$Q \times 10^{26}$ [esu/cm^2]	0.637	1.4	0	2.5	4.3
d_k [nm]	0.289	0.364	0.38	0.376	0.33
T_r (at 298 K) = T/T_c	8.98	2.36	1.57	2.24	0.98

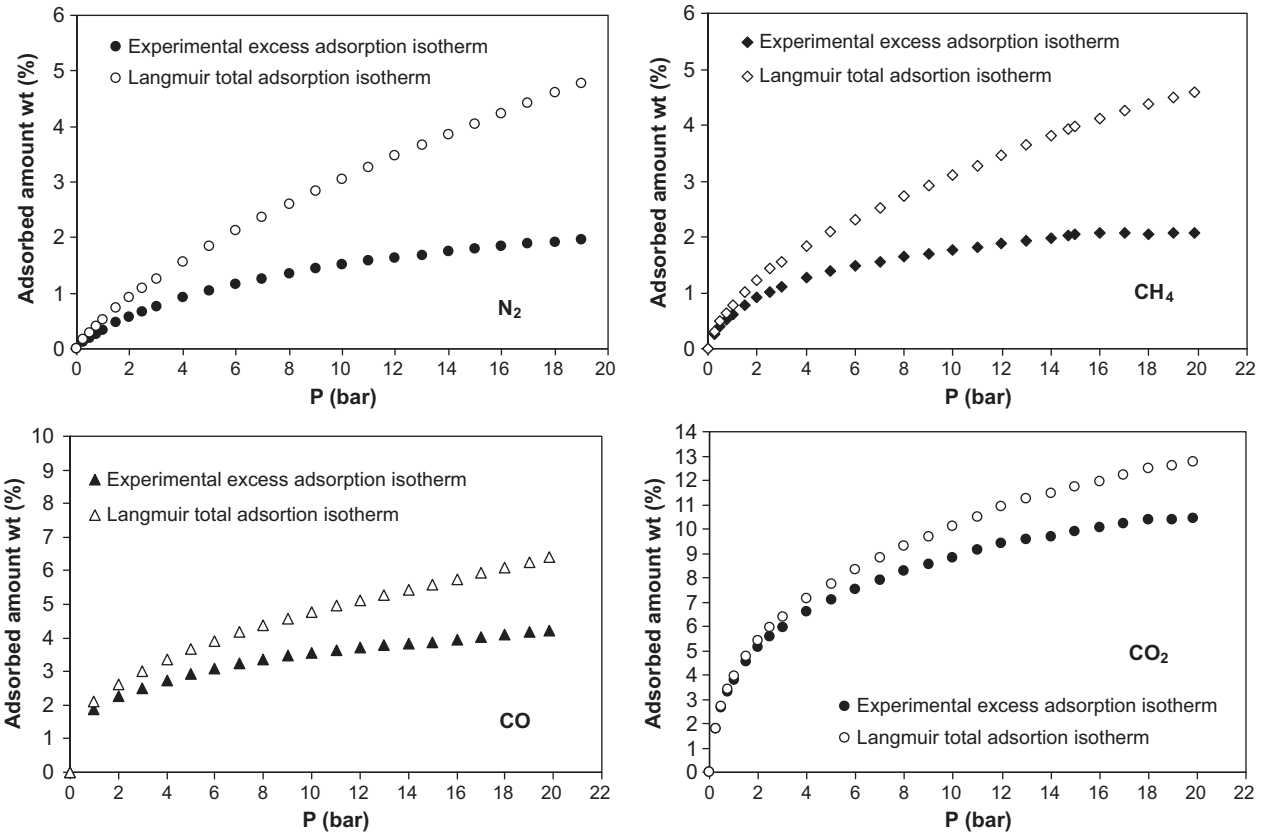

Fig. 5. Experimental excess adsorption isotherms and calculated total adsorption isotherms of N_2, CH_4, CO and CO_2 at 298 K. The Langmuir model has been adopted for the description of the total adsorption isotherms at the pressure range of the measurements.

atures is sufficiently larger than that found at room temperature. It is obviously due to the fact that low temperature reinforces the gas–gas and gas–adsorbent particle attractive interactions. In our case, the temperature (298 K) of the adsorption isotherms of H_2, N_2, CH_4 and CO gases is quite higher than their critical ones, whereas for CO_2 is nearly equal. Therefore, by considering the experimental excess as well as the corrected total (or absolute) adsorption results from Figs. 4 and 5, respectively, we come to the conclusion that the adsorption isotherms of these gases obtained are realistic and the wt% gas adsorbed shows characteristic differences from one gas to another as expected. From these figures, we may observe that the adsorption capability for the aforementioned gases is restricted and increases in the following order: $H_2 \ll N_2 \approx CH_4 < CO \ll CO_2$.

The gravimetric excess and absolute adsorption uptake for CH_4 with pressure exhibits almost a similar behavior to that of N_2 and lower values compared to CO, despite the lower reduced temperature of the former gas, which indicates the existence of weaker interactions with the substrate in comparison with the two other gases. Furthermore, the substantially higher uptake of CO under the same thermodynamic conditions reflects the strength of interaction with the substrate due possibly to the higher quadrupole interaction energy. Note that the investigated gases, with the exception of CO, have no dipole moment, whereas N_2, CO, CO_2 and H_2 possess relatively high quadrupole moment, which gives rise to additional interactions among the specific moment and the substrate (SWCNTs). Moreover, in the case of CO_2 which is the studied adsorbate with the highest quadrupole moment, the effect of the subcritical adsorption temperature and the smaller kinetic diameter (d_k = 0.33 nm) compared to the other adsorbates (except for H_2) should account for the highest measured adsorption capacity for the specific gas (10.42 wt% at 1.98 MPa). By inspecting the H_2 isotherm, as shown in Fig. 4 the excess adsorption of this adsorbate with pressure up to 1.8 MPa appears to be the lowest one compared to other studied gases. In this particular case, the effect of the very high supercritical adsorption temperature (298 K $\approx 9T_{c,H_2}$) and the relatively small quatrupole moment of the molecule compared to the other gases from Table 3 (except CH_4 which exhibits an octopole as the first no vanished moment) should account for this adsorption result.

5.2. GCMC simulation results

One of the main goals of this work has been the estimation via computer simulation of the adsorption capacity of the aforementioned gases in SWNTs with open end caps and approximately similar geometric characteristics with those used in the conducting gravimetric adsorption experiment.

As a first result, we present in Fig. 6 the calculated chemical potentials, μ, of the pure gases obtained from MC NPT simulations. We may see from this figure that in the case of CH_4 the simulations were carried out at 273 and 298 K. In addition, all the simulations were performed up to 20 bars, except the case of H_2 and CO_2 whereas the calculations were extended up to 100 and 60 bars, respectively. By inspecting the results obtained as a function of pressure, we may observe substantial differences between the investigated gases as expected. We recall here that, for this task we used the well-established Widom's [55] test particle method and our predictions are in successful agreement with previous relevant studies.

Further to the simulation results, the molecular gases are mainly adsorbed in the internal space of the tubes (intertube space), as it can also be clearly seen from representative snapshots (see for instance Fig. 3 for CO_2), an outcome presumably due to a quite close packing modeling of the tube arrays employed in the simulations.

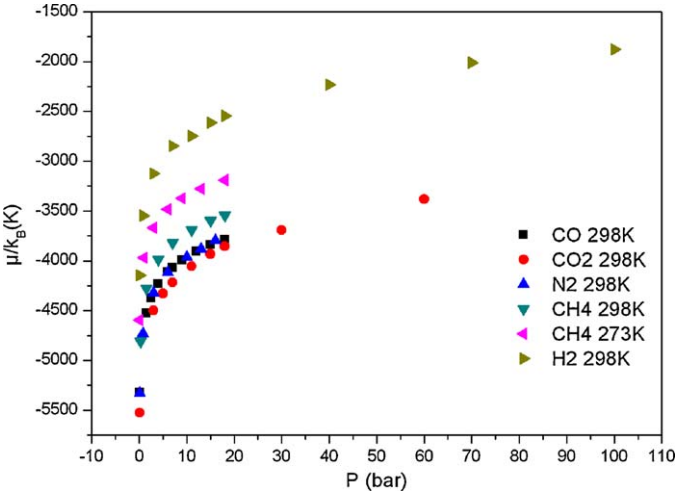

Fig. 6. Chemical potential of the gases studied as a function of the pressure from NPT MC simulations.

For the calculation of the wt% adsorption uptake isotherms, the following commonly parameters were calculated. First of all, for the calculation of the gravimetric storage capacity, ρ_w, defined as the absolute value adsorption per mass of adsorbent from Eq. (18), we took into account that the total weight of the system is the sum of the NTs weight plus the gas weight. In our case, each NT consists of 504 carbon atoms and there are 9 CNTs in the simulation cell.

$$\rho_w = \frac{N_{gas} m_{gas}}{N_{gas} m_{gas} + N_c m_c} \tag{18}$$

where N_{gas} and N_c are the number of gas molecules and carbon atoms in the simulation box, and m_{gas}, m_c are the molar mass, respectively. In each case, the number of the gas molecules in the simulation box at equilibrium is obtained from the GCMC runs and from that it is trivial to further calculate the weight percentages.

The simulated and experimental adsorption isotherms of 298 K for the gases studied here are presented in Fig. 7. From these figures we may observe that the simulated amount of the adsorbed gases show a similar trend with experiment, namely follows the order $CO_2 > CO > N_2$, $CH_4 > H_2$, which is in excellent agreement with experiment. We have to mention however that, in each case the simulated adsorption isotherm overestimates somewhat the corresponding experimental one. To this fact, we may assume that the difference in the uptake values can be ascribed to a number of possible factors among them we mention the following ones: (i) to the employed model calculations, (ii) to the possible remained carbonaceous impurities in the sample, and (iii) to a proportion of close ended tubes, even contained in the experimental sample after preparation (Fig. 8).

In order to obtain a detailed picture at molecular level of how the adsorbed gases are distributed inside the CNTs, we have calculated the density profiles of the adsorbed gas for each system under investigation. We used the concentric cylindrical shells histogram method for the calculation of this property, starting from the center of the simulation box, which coincides with the geometrical center

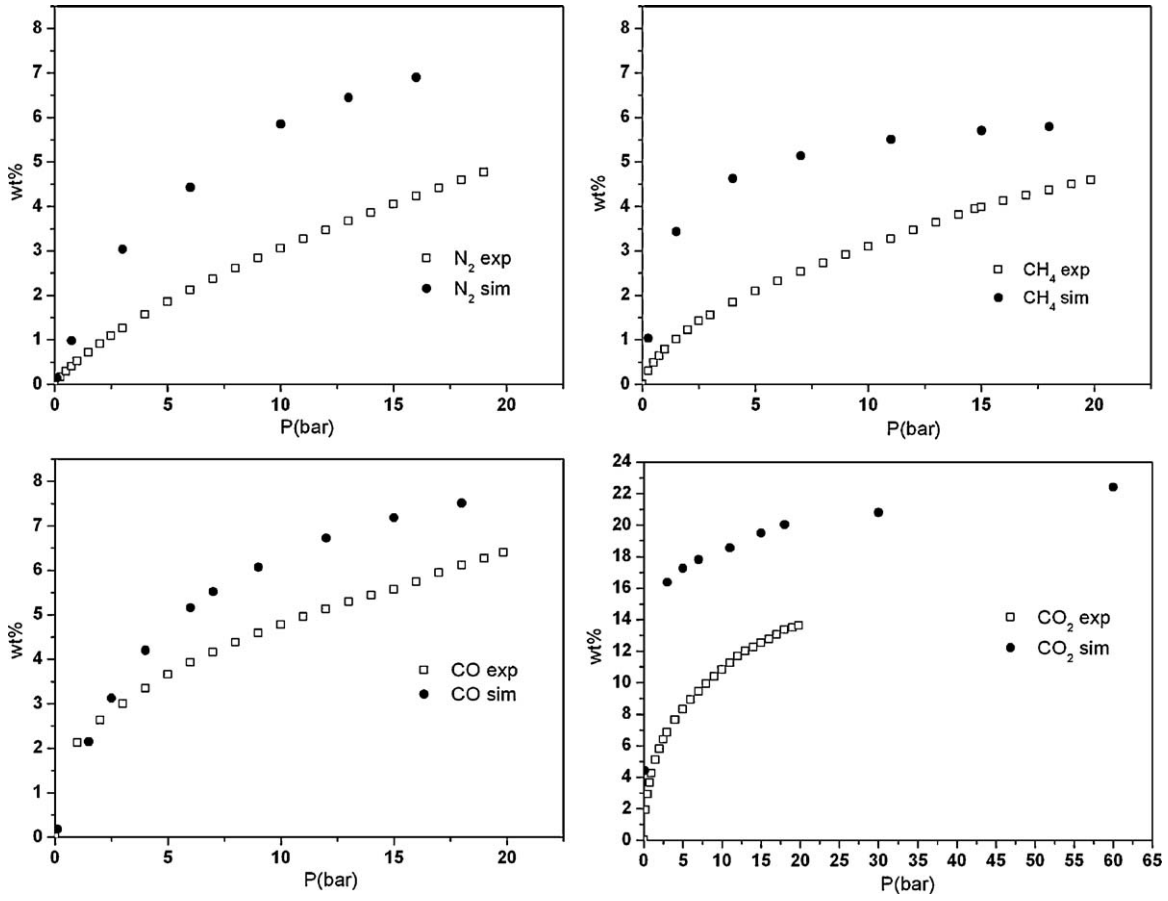

Fig. 7. Experimental and simulated total (or absolute) adsorption isotherms of the gases, N_2, CH_4, CO and CO_2 at 298 K from this study, in a direct comparison. The Langmuir model has been adopted for the description of the adsorption isotherms obtained in the pressure range examined.

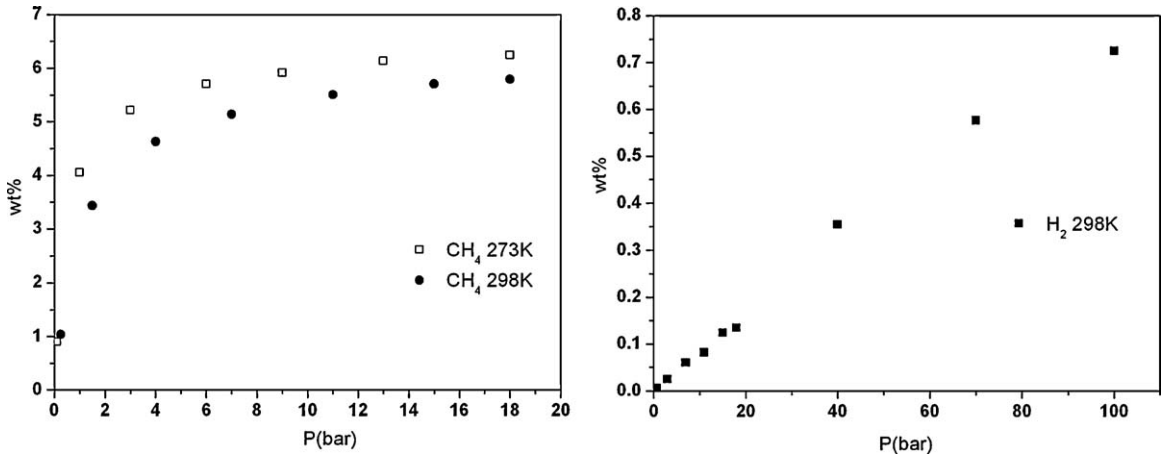

Fig. 8. The simulated total (or absolute) adsorption isotherms for CH_4 of 273 and 298 K in comparison and, for H_2 of 298 K up to 100 bars from this study.

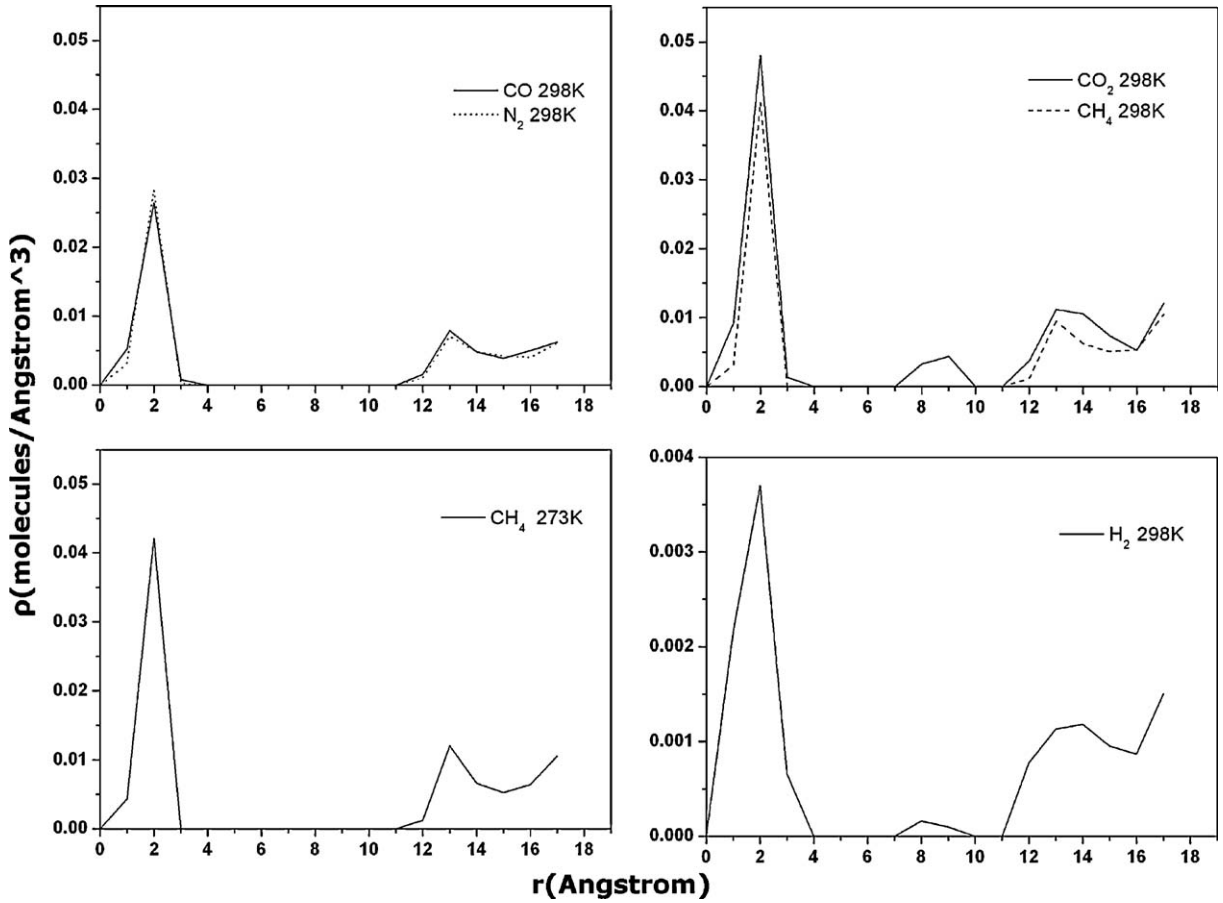

Fig. 9. Density profiles of the adsorbed gases in (9, 9) SWCNTs model from GCMC simulations in this work at 298 K except methane (bottom left) which is at 273 K.

of the central tube (Figs. 3 and 9). By inspecting the corresponding diagrams from Fig. 9, we may easily observe that a large amount of the adsorbed gases is found inside the tube near the wall surface, while gas molecules around the symmetry axis of the tube is significantly of smaller amount.

Finally, for a visual perspective of the physisorption phenomenon of gas molecules in the aforementioned SWNTs model, we have selected and carefully elaborated some snapshots of representative configurations emphasizing the amount and the distribution profile of the adsorbed particles inside the SWNTs surfaces.

6. Concluding remarks

In the present work, experimental as well as GCMC simulation techniques were employed in order to investigate the adsorption phenomenon of various gases in SWCNTs. The gases that were studied were CO_2, CO, N_2, CH_4 and H_2 and the temperature chosen 298 K.

The pristine SWCNTs material used in this study had a nominal distribution of outer diameters and length distribution. Prior to the adsorption gas experiment, we employed an oxidation process with the aim to remove amorphous carbon impurities as well as

to open if possible partial closed SWCNTs hemispherical caps. The porous structure of the oxidized–annealed sample was examined by means of N_2 porosimetry. An IGA gravimetric adsorption apparatus was employed to obtain adsorption isotherms of high purity gases at 298.15 K. The equilibrium pressures ranged from 0.01 up to 1.9 MPa in the case of H_2 and N_2 and up to 2.0 MPa for CH_4, CO and CO_2. Upon completion of degassing, the initial sample mass was measured. Afterwards, the sample chamber was thermally equilibrated at the temperature of measurements and appropriate gas pressure increments were released into the chamber to reach the selected equilibrium pressures. The increase of sample mass due to adsorption was continuously recorded until equilibrium of the adsorption system was attained and then, the final mass of adsorbent plus adsorbate was obtained.

The employment of the GCMC atomistic simulation technique can investigate the storage capacity in terms of the weight percentage, wt%, of the adsorbed material in large-scale NT systems at different thermodynamic conditions (P, T), as proposed in numerous previous studies. According to this, in the framework of this study the experimental procedure was combined with GCMC simulations of the systems and the results obtained were compared and discussed.

Both the experimental and simulated total (or absolute) adsorption isotherms show the same qualitative behavior of the adsorption in SWCNTs, with the most favorable gas for adsorption at these thermodynamic conditions to be CO_2 and the least one to be H_2. The density profiles obtained from the simulation show that almost all the gas adsorbed molecules are distributed inside and near the pore walls as the CNTs are close packed together and there is not enough space in the interstitial channels. The difference in the amount of the adsorbed gases between the two aforementioned techniques has been discussed and is attributed to a number of real factors among them the impurities in the sample that was measured experimentally.

Acknowledgments

The authors would like to thank V. Kouvelos for providing technical support on the experimental part of this work. Financial support by European Social Fund, the Greek General Secretariat of Research and Techology (PENED project 03ED181) and OSEO, France through the QMatInfo project are gratefully acknowledged.

Appendix A. Supplementary data

Supplementary data associated with this article can be found, in the online version, at doi:10.1016/j.supflu.2010.09.017.

References

[1] S. Hynek, W. Fuller, J. Bentley, Hydrogen storage by carbon sorption, International J. Hydrogen Energy 22 (1997) 601–610.
[2] S. Iijima, Helical microtubules of graphitic carbon, Nature 354 (1991) 56–58.
[3] G. Che, B.B. Lakshmi, C.R. Martin, E.R. Fisher, R.S. Ruoff, Chemical vapor deposition based synthesis of carbon nanotubes and nanofibers using a template method, Chemistry of Materials 10 (1998) 260–267.
[4] K.P. De Jong, J.W. Geus, Carbon nanofibers: catalytic synthesis and applications, Catalysis Reviews: Science and Engineering 42 (2000) 481–510.
[5] A.C. Dillon, K.M. Jones, T.A. Bekkedahl, C.H. Kiang, D.S. Bethune, M.J. Heben, Storage of hydrogen in single-walled carbon nanotubes, Nature 386 (1997) 377–379.
[6] A. Kuznetsova, D.B. Mawhinney, V. Naumenko, J.T. Yates Jr., J. Liu, R. Smalley, Enhancement of adsorption inside of single-walled nanotubes: opening the entry ports, Chemical Physics Letters 321 (2000) 292–296.
[7] C. Saridara, S. Mitra, Chromatography on self-assembled carbon nanotubes, Analytical Chemistry 77 (2005) 7094–7097.
[8] M. Rzepka, P. Lamp, M.A. de la Casa-Lillo, Physisorption of hydrogen on microporous carbon and carbon nanotubes, J. Physical Chemistry B 102 (1998) 10894–10898.
[9] M. Dresselhaus, K.A. Williams, P.C. Eklund, Hydrogen adsorption in carbon materials, MRS Bulletin 24 (1999) 45–50.
[10] F. Darkrim, D. Levesque, Monte Carlo simulations of hydrogen adsorption in single-walled carbon nanotubes, J. Chemical Physics 109 (1998) 4981–4984.
[11] Q. Wang, J.K. Johnson, Molecular simulation of hydrogen adsorption in single-walled carbon nanotubes and idealized carbon slit pores, J. Chemical Physics 110 (1998) 577–586.
[12] Q. Wang, J.K. Johnson, Optimization of carbon nanotube arrays for hydrogen adsorption, J. Physical Chemistry B 103 (1999) 4809–4813.
[13] S.M. Lee, Y.H. Lee, Hydrogen storage in single-walled carbon nanotubes, Applied Physics Letters 76 (2000) 2877–2879.
[14] S.M. Lee, K.H. An, Y.H. Lee, G. Seifert, T. Frauenheim, Novel mechanism of hydrogen storage in carbon nanotubes, J. Korean Physical Society 38 (2001) 686–692.
[15] S.M. Lee, K.H. An, Y.H. Lee, G. Seiffert, T. Frauenheim, A hydrogen storage mechanism in single-walled carbon nanotubes, J. American Chemical Society 123 (2001) 5059–5063.
[16] A. Züttel, P. Sudan, P. Mauron, T. Kiyobayashi, C. Emmenenrgger, L. Schlapbach, Hydrogen storage in carbon nanostructures, International J. Hydrogen Energy 27 (2002) 203–212.
[17] C. Gu, G.H. Gao, Y.X. Yu, Density functional study of the adsorption and separation of hydrogen in single-walled carbon nanotube, International J. Hydrogen Energy 29 (2004) 465–473.
[18] G. Mpourmpakis, G.E. Froudakis, G.P. Lithoxoos, J. Samios, Effect of curvature and chirality for hydrogen storage in single-walled carbon nanotubes: a combined ab initio and Monte Carlo investigation, J. Chemical Physics 126 (2007), 144704 1-10.
[19] F.L. Darkrim, P. Malbrunot, G.P. Tartaglia, Review of hydrogen storage by adsorption in carbon nanotubes, International J. Hydrogen Energy 27 (2002) 193–202.
[20] V. Meregalli, M. Parrinello, Review of theoretical calculations of hydrogen storage in carbon-based materials, Applied Physics A: Materials Science & Processing 72 (2001) 143–146.
[21] Y. Ye, C.C. Ahn, C. Witham, B. Fultz, J. Liu, A.G. Rinzler, D. Colbert, K.A. Smith, R.E. Smalley, Hydrogen adsorption and cohesive energy of single-walled carbon nanotubes, Applied Physics Letters 74 (1999) 2307–2310.
[22] C. Liu, Y.Y. Fan, M. Liu, H.T. Cong, H.M. Cheng, M.S. Dresselhaus, Hydrogen storage in single-walled carbon nanotubes at room temperature, Science 286 (1999) 1127–1129.
[23] H.W. Zhu, L.J. Ci, A. Chen, Z.Q. Mao, C.L. Xu, X. Xiao, et al., Hydrogen energy progress XIII, in: Proceedings of the 13th World Hydrogen Energy Conference, International Association for Hydrogen Energy, Beijing, China, 2000, p. 560.
[24] X.B. Wu, P. Chen, J. Lin, K.L. Tan, Hydrogen uptake by carbon nanotubes, International J. Hydrogen Energy 25 (2000) 261–265.
[25] G.E. Ioannatos, X.E. Verykios, H_2 storage on single- and multi-walled carbon nanotubes, International J. Hydrogen Energy 35 (2010) 622–628.
[26] G. Mpourmpakis, G.E. Froudakis, G.P. Lithoxoos, J. Samios, SiC. Nanotubes:, A novel material for hydrogen storage, Nano Letters 6 (2006) 1581–1583.
[27] G.P. Lithoxoos, J. Samios, Y. Carissan, Investigation of silicon model nanotubes as potential candidate nanomaterials for efficient hydrogen storage: a combined ab initio/grand canonical Monte Carlo simulation study, J. Physical Chemistry C 112 (2008) 16725–16728.
[28] H. Cheng, A.C. Cooper, G.P. Pez, M.K. Kostov, P. Piotrowski, S.J. Stuart, Molecular dynamics simulations on the effects of diameter and chirality on hydrogen adsorption in single walled carbon nanotubes, J. Physical Chemistry B 109 (2005) 3780.
[29] H. Kajiura, S. Tsutsui, K. Kadono, M. Kakuta, M. Ata, Y. Mrakami, Hydrogen storage capacity of commercially available carbon materials at room temperature, Applied Physics Letters 82 (2003) 1105.
[30] S.M. Lee, S.-H. Park, S.C. Lee, H.J. Kim, Adsorption properties of N_2, H_2 on single-walled carbon nanotubes modified by KOH, Chemical Physics Letters 432 (2006) 518.
[31] J. Miyawaki, K. Kaneko, Pore width dependence of the temperature change of the confined methane density in slit-shaped micropores, Chemical Physics Letters 337 (2001) 243–247.
[32] M.M.K. Salem, P. Braeuer, M. Szombathely, M. Heuchel, P. Harting, K. Quitzsch, M. Jaroniec, Thermodynamics of high-pressure adsorption of argon, nitrogen and methane on microporous adsorbents, Langmuir 14 (1998) 3376–3389.
[33] A Kuznetsova, J.J.T. Yates, J. Liu, R.E. Smalley, Physical adsorption of xenon in open single walled carbon nanotubes: observation of a quasi-one-dimensional confined Xe phase, J. Chemical Physics 112 (2000) 9590–9598.
[34] D.-H. Yoo, G.-H. Rue, M.H.W. Chan, Y.-H. Hwang, H.-K. Kim, Study of nitrogen adsorbed on open-ended nanotube bundles, J. Physical Chemistry B 107 (2003) 1540–1542.
[35] S. Brunauer, P.H. Emmett, E. Teller, Adsorption of gases in multimolecular layers, J. American Chemical Society 60 (1938) 309–319.
[36] M.M. Dubinin, The potential theory of adsorption of gases and vapors for adsorbents with energetically nonuniform surfaces, Chemical Reviews 60 (1960) 235–241.
[37] M.M. Dubinin, Adsorption in micropores, J. Colloid and Interface Science 23 (1967) 487–499.
[38] K. Kaneko, Determination of pore size and pore size distribution: 1. Adsorbents and catalysts, J. Membrane Science 96 (1994) 59–89.
[39] N.D. Hutson, R.T. Yang, Theoretical basis for the Dubinin–Radushkevitch (D–R) adsorption isotherm equation, Adsorption 3 (1997) 189–195.

[40] P.J.M. Carrot, R.A. Roberts, K.S.W. Sing, Adsorption of nitrogen by porous and non-porous carbons, Carbon 25 (1987) 59–68.
[41] M.M. Dubinin, V.A. Astakhov, Description of adsorption equilibria of vapors on zeolites over wide ranges of temperature and pressure, in: Advances in Chemistry Series, vol. 102, 1971, pp. 69–85 (Chapter 44).
[42] A. Kapoor, J.A. Ritter, R.T. Yang, On the Dubinin–Radushkevich equation for adsorption in microporous solids in the Henry's law region, Langmuir 5 (1989) 1118–1121.
[43] H.F. Stoeckli, Microporous carbons and their characterization: the present state of the art, Carbon 28 (1990) 1–6.
[44] M. Kruk, M. Jaroniek, J. Choma, Comparative analysis of simple and advanced sorption methods for assessment of microporosity in activated carbons, Carbon 36 (1998) 1447–1458.
[45] P.G. Menon, Adsorption at high pressures, Chemical Reviews 68 (1968) 277–294.
[46] F. Darkrim, J. Vermesse, P. Malbrunot, D. Levesque, Monte Carlo simulations of nitrogen and hydrogen physisorption at high pressures and room temperature. Comparison with experiments, J. Chemical Physics 110 (1999) 4020–4027.
[47] A.M. Czerny, P. Bénard, R. Chahine, Adsorption of nitrogen on granular activated carbon: experiment and modeling, Langmuir 21 (2005) 2871–2875.
[48] L. Zhou, Y. Zhou, S. Bai, Ch. Lü, B. Yang, Determination of the adsorbed phase volume and its application in isotherm modeling for the adsorption of supercritical nitrogen on activated carbon, J. Colloid and Interface Science 239 (2001) 33–38.
[49] A. Herbst, P. Harting, Thermodynamic description of excess isotherms in high-pressure adsorption of methane, argon and nitrogen, Adsorption 8 (2002) 111–123.
[50] K Murata, M. El-Merraoui, K. Kaneko, A new determination method of absolute adsorption isotherm of supercritical gases under high pressure with a special relevance to density-functional theory study, J. Chemical Physics 114 (2001) 4196–4205.
[51] S. Gumma, O. Talu, Gibbs dividing surface and Helium adsorption, Adsorption 9 (2003) 17–28.
[52] D.D. Do, H.D. Do, Adsorption of argon from sub- to supercritical conditions on graphitized thermal carbon black and in graphitic slit pores: a grand canonical Monte Carlo simulation study, J. Chemical Physics 123 (2005) 0847011–08470115.
[53] L. Zhan, K.X. Li, R. Zhang, Q.F. Liu, Ch.X. Lü, L.Ch. Ling, Improvements of the DA equation for application in hydrogen adsorption at supercritical conditions, J. Supercritical Fluids 28 (2004) 37–45.
[54] P. Bénard, R. Chahine, P.A. Chandonia, D. Cossement, G. Dorval-Douville, L. Lafi, P. Lachance, R. Paggiaro, E.J. Poirier, Comparison of hydrogen adsorption on nanoporous materials, J. Alloys and Compounds 446 (2007) 380–384.
[55] M. Aoshima, K. Fukasawa, K. Kaneko, Micropore filling of supercritical Xe in micropores of activated carbon fibers, J. Colloid and Interface Science 222 (2000) 179–183.
[56] G.L. Aranovich, M.D. Donohue, Adsorption isotherms for microporous adsorbents, Carbon 33 (1995) 1369–1375.
[57] G. Aranovich, M. Donohue, Determining surface areas from linear adsorption isotherms at supercritical conditions, J. Colloid and Interface Science 194 (1997) 392–397.
[58] P. Bénard, R. Chahine, Modeling of high-pressure adsorption isotherms above the critical temperature on microporous adsorbents: application to methane, Langmuir 13 (1997) 808–813.
[59] K. Murata, K. Kaneko, Nano-range interfacial layer upon high-pressure adsorption of supercritical gases, Chemical Physics Letters 321 (2000) 342–348.
[60] G.L. Deitrick, L.E. Scriven, H.T. Davis, Efficient molecular simulation of chemical potentials, J. Chemical Physics 90 (1989) 2370–2385.
[61] K. Binder (Ed.), The Monte Carlo Methods in Condensed Matter Physics, Topics in Applied Physics, vol. 71, Springer, New York, Berlin, 1995.
[62] J. Tersoff, R.S. Ruoff, Structural properties of a carbon nanotube crystal, Physical Review Letters 73 (1994) 676–679.
[63] J.P. Lu, Elastic properties of carbon nanotubes and nanoropes, Physical Review Letters 79 (1997) 1297–1300.
[64] L.A. Cirifalco, M. Hodak, R.S. Lee, Carbon nanotubes, buckyballs, ropes, and a universal graphitic potential, Physical Review B 62 (2000) 13104–13110.
[65] B Saager, J. Fischer, Predictive power of effective intermolecular pair potentials: MD simulation results for methane up to 1000 MPa, Fluid Phase Equilibria 57 (1990) 35–46.
[66] K. Makrodimitris, G.K. Papadopoulos, D.N. Theodorou, Prediction of permeation properties of CO_2 and N_2 through silicalite via molecular simulations, J. Physical Chemistry B 105 (2001) 777–788.
[67] M.B. Sweatman, N. Quirke, Modelling gas adsorption in slit-pores using Monte Carlo simulation, Molecular Simulation 27 (2001) 295–321.
[68] J.G. Harris, K.H. Yang, Carbon dioxide's liquid–vapor coexistence curve and critical properties as predicted by a simple molecular model, J. Physical Chemistry 99 (1995) 12021–12024.
[69] Scienomics Sarl, 17 Square Edouard VII 75009 Paris, France.
[70] A. Peigney, C. Laurent, E. Flahaut, R.R. Bacsa, A. Rousset, Specific surface area of carbon nanotubes and bundles of carbon nanotubes, Carbon 39 (2001) 507–514.
[71] S.J. Gregg, K.S.W. Sing, Adsorption, Surface Area and Porosity, Academic Press, London, 1967, pp. 1–34 (Chapter 1), pp. 35–120 (Chapter 2).
[72] K.A.G. Amankwah, J.S. Noh, J.A. Schwarz, Hydrogen storage on superactivated carbon at refrigeration temperatures, International J. Hydrogen Energy 14 (1989) 437–447.
[73] M.R. Johnson, S. Rolsa, P. Wass, M. Muris, M. Bienfait, P. Zeppenfeld, N. Dupont-Pavlovsky, Neutron diffraction and numerical modelling investigation of methane adsorption on bundles of carbon nanotubes, Chemical Physics 293 (2003) 217–230.
[74] S.E. Weber, S. Talapatra, C. Journet, A. Zambano, A.D. Migone, Determination of the binding energy of methane on single-walled carbon nanotube bundles, Physical Review B 61 (2000) 13150–13154.
[75] S. Talapatra, A.J. Zambano, S.E. Weber, A.D. Migone, Gases do not adsorb on the interstitial channels of closed-ended single-walled carbon nanotube bundles, Physical Review Letters 85 (2000) 138–141.
[76] M.M. Calbi, M.W. Cole, S.M. Gatica, M.J. Bojan, G. Stan, Condensed phases of gases inside nanotube bundles, Reviews of Modern Physics 73 (2001) 857–865.
[77] K.A. Williams, P.C. Eklund, Monte Carlo simulations of H_2 physisorption in finite-diameter carbon nanotube ropes, Chemical Physics Letters 320 (2000) 352–358.
[78] M.K. Kostov, M.W. Cole, J.C. Lewis, P. Diep, J.K. Johnson, Many-body interactions among adsorbed atoms and molecules within carbon nanotubes and in free space, Chemical Physics Letters 332 (2000) 26–34.
[79] G. Stan, M.J. Bojan, S. Curtarolo, S.M. Gatica, M.W. Cole, Uptake of gases in bundles of carbon nanotubes, Physical Review B 62 (2000) 2173–2180.
[80] R.S.A. de Lange, K. Keizer, A.J. Burggraaf, Analysis and theory of gas transport in microporous sol-gel derived ceramic membranes, J. Membrane Science 104 (1995) 81–100.
[81] T. Tomita, K. Nakayama, H. Sakai, Gas separation characteristics of DDR type zeolite membrane, Microporous and Mesoporous Materials 68 (2004) 71–75.
[82] L. Predescu, F.H. Tezel, S. Chopra, Adsorption of nitrogen, methane, carbon monoxide, and their binary mixtures on aluminophosphate molecular sieves, Adsorption 3 (1997) 7–25.
[83] S.K Lilov, Determination of the effective kinetic diameter of the complex molecules, Crystal Research and Technology 21 (1986) 1299–1302.
[84] I.A. Sokolova, B.E. Lusternik, Numerical Analysis and its Applications, Lecture Notes in Computer Science 1196, Springer 1997, p. 474.
[85] J. Zhang, J. Lu, W. Liu, Q. Xue, Separation of CO_2 and CH_4 through two types of polyimide membrane, Thin Solid Films 340 (1999) 106–109.